OPTICAL COHERENCE TOMOGRAPHY

TOMAŽ CVETKO

Fakulteta za matematiko in fiziko
Univerza v Ljubljani

Optical coherence tomography is a non-invasive high resolution imaging technique based on low coherence interferometry. In this paper, basic operation principle of time-domain optical coherence tomography is derived using two simplified models. Biological and medical applications are discussed, then Fourier-domain optical coherence tomography concept is introduced as a necessary improvement to enable video-rate image collection. Finally, alternative sources of contrast are discussed and integration of the Doppler principle with optical coherence tomography is described as a way to measure 3D flow velocity profiles of scattering liquids.

OPTIČNA KOHERENČNA TOMOGRAFIJA

Optična koherenčna tomografija je neinvazivna tehnika slikanja z visoko ločljivostjo, ki temelji na nizkokoherenčni interferometriji. V članku je izpeljan osnovni način delovanja v časovni domeni na podlagi dveh poenostavljenih modelov. V drugem delu se članek ukvarja z uporabo metode v biološke in medicinske namene, vpeljana je optična koherenčna tomografija v Fourierovi domeni kot potrebna izboljšava za hitrejši zajem slik. V zadnjem poglavju se članek posveča alternativnim virom kontrasta v slikah z optično koherenčno tomografijo in predstavljeno je, kako se lahko uporabi Dopplerjev princip za meritev tridimenzionalnih profilov hitrosti v sipajočih tekočinah.

1. Introduction

Optical coherence tomography (OCT) was developed in the late 1980s and early 1990s as a technique for tomographic imaging of biological tissues. From the early stages on, OCT has shown great potential for medical applications. After three decades of intensive research, OCT is now a mature, commercially available technology, routinely used in ophthalmology, cardiology, dermatology and other medical specialties, as well as in other, non-medical fields.

Optical coherence tomography uses light-wave "echoes" originating from reflections and scattering inside a sample to determine its internal structure. In this aspect OCT is analogous to ultrasound imaging, which can serve as an instructive comparison. While ultrasound image contrast emerges from reflections of acoustic waves (mechanical deformation), OCT exploits reflections of electromagnetic waves (light) to produce contrast. Because the speed of light is much larger than the speed of sound, direct time-of-flight measurements (as in ultrasound imaging) are not feasible. Instead, OCT uses coherence gating to determine the depth from which the echoes originated. Penetration depth and image resolution also differ greatly between the two methods. While ultrasound images have spatial resolutions below 1 mm and penetration depths of up to $\sim 10\,\mathrm{cm}$, OCT routinely achieves resolutions around $10\,\mu\mathrm{m}$ but has imaging depth of a couple of millimeters. Because OCT has better resolution than ultrasound, but achieves lower imaging depths, optical coherence tomography is complementary to ultrasound imaging.

Comparing OCT to other medically important imaging techniques leads to similar conclusions. Confocal microscopy achieves resolutions of around $1\,\mu\mathrm{m}$, but has significantly lower imaging depth than OCT. Therefore OCT fills the gap between microscopy, which has imaging depth limitations, and other imaging techniques (ultrasound, X-ray, CT, MRI, etc.), which are limited by their image resolution [1, 2]. This unique position of OCT among imaging techniques caused great interest in the medical community as well as quick commercialization. In the late 1990s and early 2000s growth in the field of OCT was almost exponential. The number of publications in a year increased tenfold in a span of 8 years, and the market for OCT equipment grew by 30% each year [2].

OCT is most widely used in ophthalmology, because it enables noninvasive examination of the internal structure of the retina, which is otherwise inaccessible. Other medical applications include

imaging of blood vessels and other intravital imaging conducted through endoscopes, mainly to search for symptoms of disease in the tissue or even detect precancerous changes. OCT is used in industry as well, especially where accurate surface or thickness measurements are required in a non-invasive and non-contact manner.

2. Theoretical background

2.1 Interferometry

Basic concepts of OCT can be presented by studying the Michelson interferometer, which consists of two mirrors and a beamsplitter [3]. We name one mirror reference (R) and other mirror sample (S) as shown in Figure 1a. With z_{R} and z_{S} we measure the distance from the beamsplitter to the sample and reference mirror, respectively.

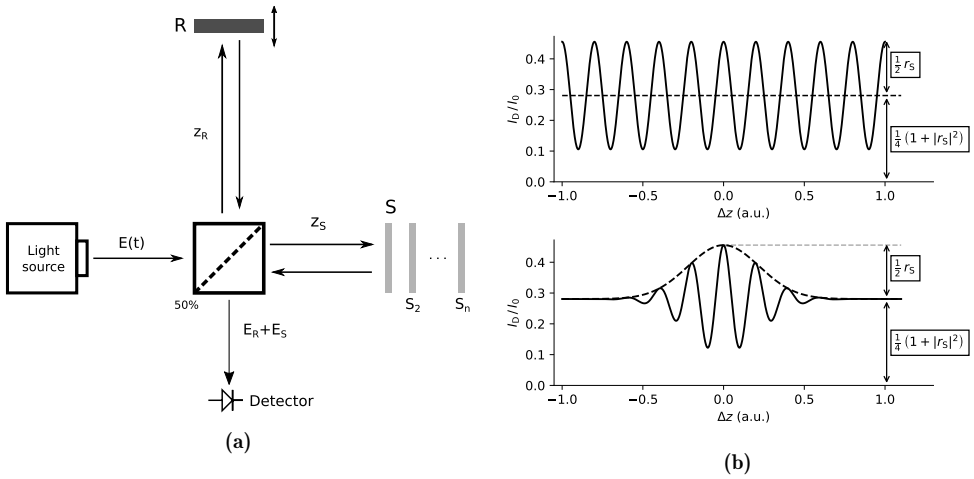

Figure 1. (a): Experimental setup: Michelson interferometer and a detector. Biological tissue can be modelled using several discrete, partial reflecting mirrors S_n. **(b)**: Detector current vs. path length difference for a monochromatic light source *(top)* and a broad band light source for $r_{\mathrm{S}} = 0.35$ *(bottom)*. Based on [1].

Light wave emitted from the light source is described with its electric field $E(z,t)$. Let us assume that the beamsplitter divides optical power equally between the two arms of the interferometer. Let mirror R be perfectly reflective ($r_{\mathrm{R}} = 1$) and mirror S have a reflection coefficient r_{S}. Light reflected in both arms is recombined at the beam splitter and directed to the detector (see Figure 1a). From now on, all equations will describe electric field at the detector and its spatial (z) dependence will be omitted.

The detector is usually a fast photodiode, which converts absorbed photons into electric current. Detector output signal is proportional to the light intensity $j(t) = \frac{1}{2}\sqrt{\epsilon}\epsilon_0 c_0 |E(t)|^2$, where ϵ is the relative permittivity of medium, ϵ_0 is the vacuum permittivity and c_0 is the speed of light in vacuum. For derivation, units are not important and from now on, optical intensity or intensity will refer to $I(t) = |E(t)|^2$. All detectors have finite response times and signal is proportional to the time averaged intensity

$$I_{\mathrm{D}}(t) = \langle |E(t)|^2 \rangle = \frac{1}{T_{\mathrm{D}}} \int_{t-T_{\mathrm{D}}}^{t} E\left(t'\right) E^*\left(t'\right) \mathrm{d}t' \ , \tag{1}$$

where T_{D} marks the response time of the detector and the brackets $\langle\rangle$ denote averaging over time. In the following derivation, explicit time dependence of the time-averaged intensity is suppressed for clarity - it turns out that time dependence of I_D is irrelevant.

In the Michelson interferometer, electric field at the detector is a sum of electric fields from the reference and sample arms and the detector signal is expressed as

$$I_{\mathrm{D}} = \langle |E_{\mathrm{R}}(t) + E_{\mathrm{S}}(t)|^2 \rangle = \\ = \langle |E_{\mathrm{R}}(t)|^2 \rangle + \langle |E_{\mathrm{S}}(t)|^2 \rangle + \langle E_{\mathrm{R}}(t) E_{\mathrm{S}}^*(t) + E_{\mathrm{R}}^*(t) E_{\mathrm{S}}(t) \rangle \ . \tag{2}$$

Because E_{R} and E_{S} were both emitted from the same light source, they can be expressed in terms of the source field before the beamsplitter, $E(t)$. Because E_{R} passes through the beamsplitter twice, the reference field at the detector is $E_{\mathrm{R}}(t) = \frac{1}{2} E(t + \tau_{\mathrm{R}})$. Compared to the reference field, the sample field has a modified amplitude and a different time delay,

$$E_{\mathrm{S}}(t) = \frac{1}{2} r_{\mathrm{S}} E(t + \tau_{\mathrm{S}}) \ . \tag{3}$$

Here, $\tau_{\mathrm{R}} = 2z_{\mathrm{R}}/c$ and $\tau_{\mathrm{S}} = 2z_{\mathrm{S}}/c$ denote the time delays in the reference and the sample arm, respectively. Let τ represent the relative time delay of the reference arm compared to the sample arm, $\tau = 2\Delta z/c$, where $\Delta z = z_{\mathrm{R}} - z_{\mathrm{S}}$ is the geometrical difference between the two arm lengths. Inserting Eq. (3) into Eq. (2) gives

$$I_{\mathrm{D}}(\tau) = \frac{1}{4} \langle |E(t)|^2 \rangle \left(1 + |r_{\mathrm{S}}|^2 \right) + \frac{1}{2} \mathrm{Re} \left[r_{\mathrm{S}} \langle E(t) E^*(t + \tau) \rangle \right] \ . \tag{4}$$

Example Lasers emit nearly monochromatic light, which is described with electric field $E_{\mathrm{wave}}(t) = E_0 \exp(-\mathrm{i}\omega t)$. The signal in Eq. (4) then simplifies to

$$I_{\mathrm{D}}(\tau) = \frac{1}{4} I_0 \left(1 + |r_S|^2 \right) + \frac{1}{2} I_0 r_{\mathrm{S}} \cos(\omega \tau) \ , \tag{5}$$

where $I_0 = |E_0|^2$. Note that I_D is only a function of the arm length difference and is constant in time. We say that oscillations of the signal intensity (see Figure 1b) continue even for large τ because lasers are *coherent* light sources. It is important to realize that there is no way of determining the equidistant position ($\tau = 0$) from the interference pattern alone.

2.1.1 Low-coherence interferometry

Consider again Eq. (4). Let us assume that the intensity fluctuations are averaged out within the detector response time. Then, time-averaging over infinity yields the same result as time-averaging over detector response time and we can introduce

$$G(\tau) = \lim_{T \to \infty} \frac{1}{T} \int_{-T/2}^{T/2} E(t) E^*(t + \tau) \, \mathrm{d}t \ . \tag{6}$$

Function $G(\tau)$ is the autocorrelation function of electric field $E(t)$, and describes how the electric field correlates with itself when delayed by τ. For all realistic light sources, the autocorrelation function vanishes for $\tau \to \infty$. Coherence time τ_{c} may thus be informally defined as the time delay at which the autocorrelation function becomes small. The corresponding coherence length is then given by $l_{\mathrm{c}} = \tau_{\mathrm{c}} c$.

When the assumptions about the time-averaging are applied to Eq. (4), any time dependence is integrated out and intensity at the detector simplifies to

$$I_{\mathrm{D}}(\tau) = \frac{1}{4} I_0 \left(1 + |r_{\mathrm{S}}|^2 \right) + \frac{1}{2} \mathrm{Re} \left[r_{\mathrm{S}} G(\tau) \right] \ , \tag{7}$$

where $I_0 = G(0) = \langle |E(t)|^2 \rangle$ is intensity of the light source. Detector signal has a constant offset, which depends on the light source intensity I_0 and reflectivity of the sample mirror, $R_{\mathrm{S}} = |r_{\mathrm{S}}|^2$.

More importantly, the second term in Eq.(7) depends on both $\tau = 2\Delta z/c$ and the light-source autocorrelation function, $G(\tau)$.

From the signal shape for a laser Eq. (5), we concluded that it contains no information about the sample mirror position. On the other hand, light sources with much broader spectra produce interference patterns only in the vicinity of the equidistant position, $z_\mathrm{R} \approx z_\mathrm{S}$. This observation is quantified in the Wiener-Khinchin theorem, which states that the field autocorrelation function $G(\tau)$ is inverse Fourier transform of the light source spectrum [4]

$$G(\tau) = \int_{-\infty}^{\infty} S(\omega) e^{\mathrm{i}\omega\tau}\,\mathrm{d}\omega \ . \tag{8}$$

From the theory of Fourier transform it is clear that, in order to achieve a confined $G(\tau)$, the spectrum $S(\omega)$ should be sufficiently broad. Specifically, if we approximate the spectrum with a Gaussian function

$$S(\omega) \propto e^{-(\omega-\omega_0)^2/2\sigma_\omega^2} \ , \tag{9}$$

then the real part of the autocorrelation function is also Gaussian, but modulated with frequency ω_0

$$\mathrm{Re}\left[G(\tau)\right] \propto e^{-\tau^2/2\sigma_\tau} \cos(\omega_0\tau) \ , \tag{10}$$

where $\sigma_\tau = \frac{1}{\sigma_\omega}$. The coherence time τ_c is defined as HWHM of the autocorrelation function envelope, $G(\tau_c) = \frac{1}{2}G(0)$. Using τ_c explicitly, the real part of the autocorrelation function is rewritten as

$$\mathrm{Re}\left[G(\tau)\right] \propto e^{-4\ln 2\left(\frac{\tau}{2\tau_c}\right)^2} \cos(\omega_0\tau) \ . \tag{11}$$

Consequently, the coherence length can be expressed as

$$l_\mathrm{c} = \frac{2\ln 2}{\pi}\frac{\lambda_0^2}{\Delta\lambda} \ , \tag{12}$$

where λ_0 is the center wavelength of the spectrum and $\Delta\lambda$ is the FWHM of the light source spectrum [1].

Experimentally, $I_\mathrm{D}(\tau)$ can be measured easily by moving the reference mirror R. Recall that $\tau = 2\Delta z/c$ and Δz changes with z_R. After inserting Eq. (11) into Eq. (7), we notice that the interference signal is spatially confined to an interval around $\Delta z = 0$. To retrieve spatial information, only the envelope is measured - modulation fringes are filtered out in signal processing. As can be seen in Figure 1b, detector signal has a peak with amplitude of $\frac{1}{2}r_\mathrm{S}I_0$ at $\tau = 0$, i.e. the position of the reference mirror z_R equal to z_S. Therefore, low coherence interferometry can be used as a method of measuring the unknown distance to the sample mirror, z_S.

2.2 Time-Domain OCT

The goal of OCT is to produce images of biological tissues, which are much more complex than a single mirror. The principle, however, remains the same as described in the previous section.

A simplified model can be used to show what results we might expect from an OCT scan. Assume that the sample consists of N mirrors S_n (as shown in Figure 1a), and light is partially reflected from each of them. Electric field reflected from the sample can then be written as

$$E_\mathrm{S}(t) = \frac{1}{2}\sum_{n=1}^{N} r_n E(t+\tau_n) \ , \tag{13}$$

where $E(t)$ denotes the light-source electric field and r_n is the relative amplitude of reflection at the n-th sample mirror. $\tau_n = 2z_n/c$ is the time delay of the n-th reflection, and z_n is the distance

between the n-th mirror and the beamsplitter. The reference field can be expressed in terms of the source field as $E_{\mathrm{R}}(t) = \frac{1}{2}E(t + \tau_{\mathrm{R}})$, where $\tau_{\mathrm{R}} = 2z_{\mathrm{R}}/c$. Inserting Eq, (13) into Eq. (2) gives

$$I_{\mathrm{D}}(\tau_{\mathrm{R}}) = \frac{1}{4}I_0\left(1 + \sum_{n=1}^{N}|r_n|^2\right) + \frac{1}{2}\sum_{n=1}^{N}\mathrm{Re}\left[r_n G\left(\tau_{\mathrm{R}} - \tau_n\right)\right] + \mathcal{O}\left(r_n^2\right) \ . \tag{14}$$

The signal from multiple discrete reflectors is a sum of autocorrelation functions $G(\tau)$ centered around the time delays τ_n, corresponding to the positions of each reflector. The amplitude of each term is proportional to the respective reflection amplitude, r_n, as illustrated in Figure 2a. This means that the signal corresponding to each reflection is confined around $\tau_{\mathrm{R}} \approx \tau_n$, which corresponds to $\Delta z_n = z_{\mathrm{R}} - z_n \approx 0$. In case of discrete reflectors, two peaks can be separated when their centers are more than l_{c} apart, therefore the axial resolution of the OCT scan is limited to one coherence length l_{c} of the light source (see Eq. (12)).

The described approach is called time-domain OCT (TD-OCT), because of the dependence of the signal I_{D} on the reference arm time delay τ_{R}. Measurement of detector current vs. reference arm time delay ($\tau_{\mathrm{R}} = 2z_{\mathrm{R}}/c$) is called an A-scan - terminology adopted from ultrasound imaging. In order to obtain a two-dimensional image, A-scans are performed repeatedly while moving the light beam laterally, to produce an image of the vertical cross section of the sample. An example of such image is shown in Figure 2b, where the structure of anterior segment of the eye is clearly visible [6]. This image was produced on a live human without any damage to the eye.

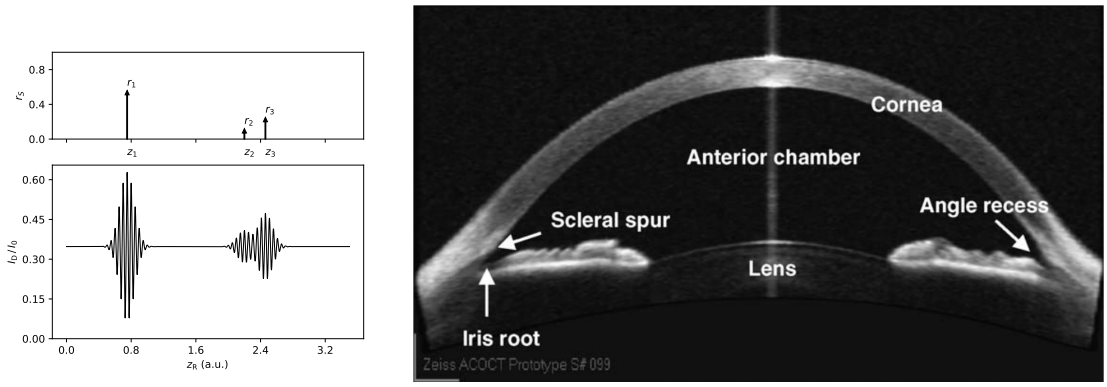

(a) **(b)**

Figure 2. **(a)**: Illustration of three partial reflecting mirrors at different locations z_n *(top)* and the corresponding OCT A-scan *(bottom)*. **(b)**: 2D OCT image of the anterior section of the eye anatomy, captured *in vivo*. Each column of the pixels represents an A-scan. Adapted from [5] and [6].

2.2.1 OCT signal from biological tissue

As implied in Section 2.2, the OCT signal is a direct consequence of light scattered back from irradiated sample. Because many sub-cellular structures in biological tissues scatter light, a realistic OCT A-scan is more complex than the one shown in Figure 2a. This means that some information can be retrieved from most volume elements of the tissue (as long as they scatter light), which is useful for an imaging technique.

Single scattering is the main source of signal in OCT. However, since multiple-scattered light lacks a well defined phase connection (coherence) with the reference beam, scattering also limits the imaging depth and the interference contrast. Scattering properties of a material are described with scattering coefficient, which is wavelength dependent. For biological tissues, scattering coefficient is usually high for visible spectrum and decreases with increasing wavelength (for example, skin has

$\mu_S \simeq 60\,\mathrm{cm}^{-1}$ at $\lambda = 500\,\mathrm{nm}$ and $\mu_S \simeq 20\,\mathrm{cm}^{-1}$ at $\lambda = 1300\,\mathrm{nm}$ [7]). Consequently, there is an important compromise between the imaging depth and OCT signal strength, when choosing the central wavelength of the light source used in OCT. Current implementations of biomedical OCT use light sources in near-infrared spectral range, with central wavelengths λ_0 at 780 - 870 nm or 1300 - 1600 nm [2].

3. Applications, improvements, limitations

3.1 Early OCT Imaging

In 1991 Huang demonstrated that OCT was applicable to examination of biological tissues [8]. They produced images *in vitro* of the peripapillary area of the retina, which is mostly transparent, and coronary artery, which is optically highly scattering tissue. Their OCT scanner was schematically equivalent to the one shown in Figure 1a, with a moving reference mirror. The light source was a superluminiscent diode (SLD) and Michelson interferometer was implemented using optical fibers, which is the standard in OCT. 17 µm resolution of the images was achieved using the central wavelength of 830 nm. The authors predicted that OCT imaging of the eye could enable reliable diagnostics of various retinal diseases, glaucoma, etc. [8].

All early devices were based on Time-Domain OCT where the reference mirror is moving during each A-scan. In addition to mechanical limitations, scan speeds are also governed by the sufficient exposure at each spatial step. Because safety standards set the maximum permissible light exposure for retinal imaging, the exposure time cannot be reduced by increasing the incident optical power. As a result, OCT images produced with this technique were susceptible to blurring due to specimen movement, which is very inconvenient for an *in vivo* imaging technique [2].

3.2 Fourier-domain OCT

Applications of the early time-domain OCT were limited by the slow imaging speeds, which stemmed from the core concept of moving the reference mirror to measure the signal $I_D(\tau_R)$. Fourier-domain OCT (FD-OCT) is an alternative approach, that does not require physical scanning in the reference arm. Instead, the idea is to measure the spectral interferogram $I_D(\omega)$ by detecting each spectral component of the signal separately. This can be achieved by replacing the photodetector in the initial setup (Figure 1a) with a spectrometer (see Figure 3a). The first implementation of FD-OCT was reported in 1995 and *in vivo* retinal imaging was demonstrated in 2002 [9]. Compared to TD-OCT, FD-OCT systems require shorter exposure times and have better sensitivity, which enabled video-rate retinal imaging *in vivo*.

Fourier transform of an arbitrary electric field $E(t)$, can be described with its Fourier transform $s(\omega) = \mathcal{F}[E(t)]$ as

$$E(t) = \int_{-\infty}^{\infty} s(\omega) e^{-\mathrm{i}\omega t}\,\mathrm{d}\omega \ . \tag{15}$$

The spectrum of electric field $E(t)$, defined as $S(\omega) = |s(\omega)|^2$, is proportional to the optical intensity in a small interval around circular frequency ω. It can be measured with a spectrometer, which consists of a diffraction grating and a linear array CCD or CMOS detector array.

Consider again the Michelson interferometer (Figure 1a) with a single mirror. The signal at one of the detectors in the spectrometer detector array consists of a single spectral component

$$I_D(\omega) = \frac{1}{4} S(\omega) \left[1 + |r_S|^2 + 2 r_S \cos\left(\omega(\tau_R - \tau_S)\right)\right] \ , \tag{16}$$

where τ_R and τ_S are the reference and the sample arm time delay, respectively. In this context, both time delays are constant and ω is the variable. For an arbitrary $S(\omega)$, Eq. (16) does not necessarily

contain any information about the location of the sample mirror. Applying inverse Fourier transform to Eq. (16) produces

$$I_{\mathrm{D}}(\tau) = \frac{1}{4}G(\tau)\left[1 + |r_{\mathrm{S}}|^2\right] + \frac{1}{4}r_{\mathrm{S}}G(\tau) * \delta(\tau \pm (\tau_{\mathrm{R}} - \tau_{\mathrm{S}}))) \ , \tag{17}$$

where $*$ denotes convolution and τ is the Fourier transform pair to ω. The Wiener-Khinchin theorem was used to replace $\mathcal{F}^{-1}(S(\omega)) = G(\tau)$. While the first term depends only on the light source and the total reflectivity of the sample, the second term consists of the sample reflectivity profile convolved with the autocorrelation function of the light source. Carrying out the convolution, we obtain the spatial FD-OCT signal

$$I_{\mathrm{D}}(\tau) = \frac{1}{4}G(\tau)\left[1 + |r_{\mathrm{S}}|^2\right] + \frac{1}{4}r_{\mathrm{S}}\left[G(\tau - (\tau_{\mathrm{R}} - \tau_{\mathrm{S}})) + G(\tau + (\tau_{\mathrm{R}} - \tau_{\mathrm{S}}))\right] \ , \tag{18}$$

which is FD-OCT equivalent of Eq. (7) [5].

Experimentally, the spectral interferogram $I_{\mathrm{D}}(\omega)$ (Eq. (16)) is measured with a spectrometer and then transformed to time-domain (Eq. (18)) using fast Fourier transform (FFT) algorithms (see Figure 3). Numerical Fourier transform of the spectral signal I_{D} effectively replaces the superposition of spectral components at the single photodetector in TD-OCT. As a result, $I_{\mathrm{D}}(\tau)$ is similar to the corresponding signal in TD-OCT (Eq. (7)), but not identical. The first term in Eq. (18) is not a constant offset as in Eq. (7), but a peak centered around $z = 0$. It is called DC artifact and is a direct consequence of using the Fourier transform instead of measuring the superposition of spectral components. Numerical signal processing of the transformed signal also allows that modulation of the autocorrelation function peaks (see Eq. (10)) is removed by taking the absolute value of the complex $\mathcal{F}^{-1}(I_{\mathrm{D}}(\omega))$.

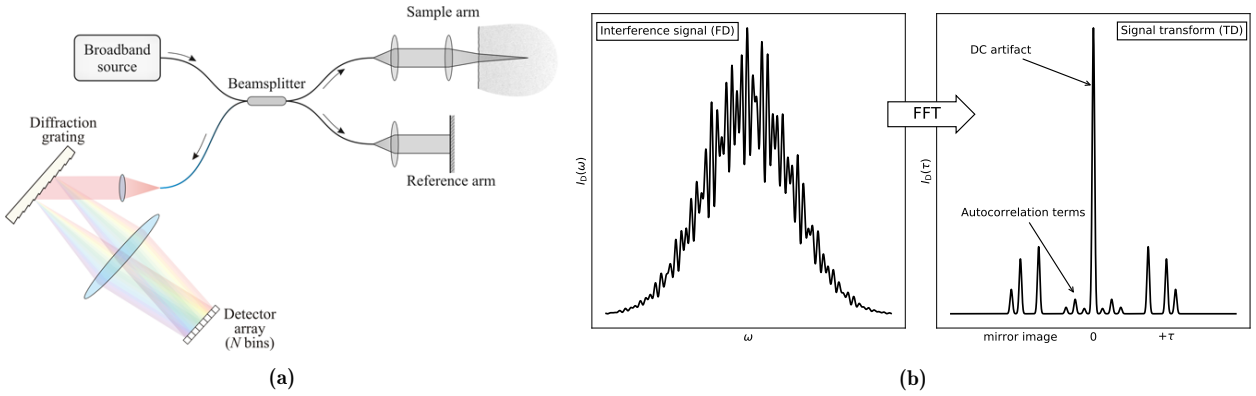

Figure 3. **(a)**: experimental setups for spectral FD-OCT. **(b)**: spectral interferogram from a sample of three mirrors. Spatial signal is then recovered by Fourier transforming into the time domain (spatial). Adapted from [10] and [11].

The time variable τ in $I_{\mathrm{D}}(\tau)$ can be interpreted as the time delay of the light $\tau = 2z/c$, where z is a spatial coordinate in the sample (the factor 2 is used because the light travels through each arm of the interferometer twice). The reflectivity profile (in this case, position of the mirror) can be estimated from the second term with resolution of coherence length l_{c}. Note that in the case of $\tau_{\mathrm{R}} = \tau_{\mathrm{S}}$, the peak representing the mirror would appear at $z = 0$ and would be covered by the DC artifact. For any other length difference of the interferometer arms $(z_{\mathrm{R}} - z_{\mathrm{S}})$, the displacement of the sample z is measured relative to the reference arm length, z_{R}. It is important to notice that the spatial signal $I_{\mathrm{D}}(\tau = 2z/c)$ is symmetrical, because the detected spectral interferogram $I_{\mathrm{D}}(\omega)$ is real so its inverse Fourier transform is Hermitian symmetric [5]. This means that the sample should

be placed on either side of the equidistant point (closer or further from the beamsplitter than z_{R}). Otherwise, $I_{\mathrm{D}}(\tau)$ overlaps with itself and this artifact cannot be removed by signal processing [5]. An illustration of how signal from multiple reflections looks like is shown in Figure 3b. In case of more complex reflectivity profiles, the signal contains additional autocorrelation terms close to $z = 0$ (peaks with amplitude $\mathcal{O}(r_n^2)$, see Eq. (14)), representing the interference between reflections in the sample. Autocorrelation terms are considered artifacts, but are usually negligible due to the much smaller reflectivity in the sample compared to the reference mirror.

3.2.1 Acquiring the interferogram

Fourier-domain OCT requires measurement of spectral interferograms $I_{\mathrm{D}}(\omega)$, equivalent to Eq. (16), but different from sample to sample. Experimentally, there are two methods of measuring such spectral interferograms.

In the spectral method, a broad-band light source is used and the photodetector is replaced with a diffraction grating and a detector array - a spectrometer (Figure 3a). All spectral components $I_{\mathrm{D}}(\omega)$ are measured simultaneously with a finite resolution in ω. From a single interferogram, the entire spatial reflectivity profile is reconstructed. This enables a 50 - 100 times increase in A-scan frequency compared to TD-OCT, which made video-grade 2D imaging and 3D volumetric imaging possible [2]. Figure 4 illustrates the advantages of FD-OCT over TD-OCT.

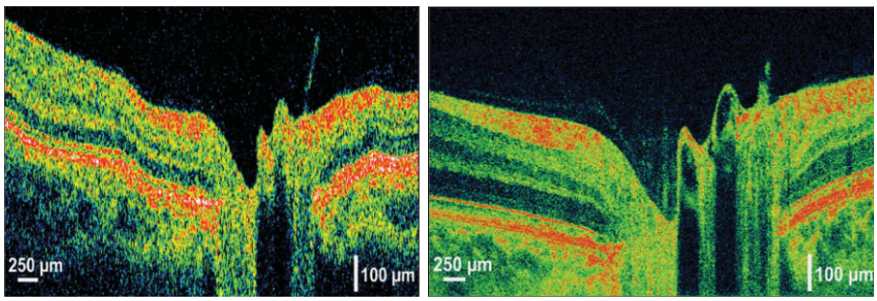

(a) **(b)**

Figure 4. Comparison of standard OCT and high-speed, ultrahigh resolution OCT using spectral Fourier domain detection. **(a)** Standard TD-OCT of the optic nerve head with $\sim 10\,\mu$m axial image resolution and 512 axial scans, acquired in ~ 1.3 s. **(b)** High-speed, ultrahigh resolution image with $\sim 2\,\mu$m axial resolution and $2,048$ axial scans, acquired in 0.13 s. Adapted from [2]

An alternative FD-OCT method uses a special light source with narrow bandwidth, which is frequency swept in time [2]. Since the frequency of the light source changes with time $\omega(t)$, interferogram $I_{\mathrm{D}}(\omega(t))$ can be measured in time while the central frequency of the light source changes which gives $I_{\mathrm{D}}(\omega)$. The resulting spectral interferogram is then Fourier transformed to the time domain (same as in the spectral method). Swept-source FD-OCT became feasible with advances in laser technology that provided suitable light sources.

Because affordable detector arrays are not available for 1300 nm and 1500 nm wavelength ranges, spectrometer-based FD method cannot be used with such wavelengths, which are (see section 2.2.1), arguably the most suitable for OCT imaging of biological tissues and organs. Meanwhile swept source FD-OCT only requires one detector. This is a major advantage over spectrometer based FD-OCT, because single detectors for the mentioned wavelength ranges are commercially available.

3.3 Limitations

From the physics standpoint, OCT capabilities and limitations are clear. Sensitivity is governed by optical power of the light source and exposure time, resolution by light source coherence length

and so on. In clinical applications, the diagnostic capabilities of OCT are not defined as clearly. In principle, when resolution of OCT systems approached that of microscopy, OCT should be directly comparable to excisional biopsy. However, many different staining methods may be used in biopsy, while contrast in OCT relies solely on different scattering properties of the investigated tissues [2]. The main limitation in medical application of OCT is therefore the fact that certain morphologies may exhibit similar optical properties and do not produce a contrast in an OCT image. As any other imaging technique, OCT is limited to detecting a single physical property of the tissue. Early studies conducted on *ex vivo* samples showed which structures in the tissue are discernible using OCT [2]. This caused rapid development of OCT imaging for those tissues and organs, where a relevant diagnostic information can be easily provided.

4. OCT extensions

Detection of changes in the tissue using OCT, especially in early stages of diseases, is limited mainly because scattering properties of the tissue are the only source of contrast. To overcome this issue, several extensions to OCT have been developed, mainly to find ways of acquiring additional information about the tissue or to provide new sources of contrast to OCT images.

Examples Multiple wavelengths can be used in order to measure spectral properties [8]. Polarization-sensitive OCT provides additional information about the light polarization changing properties of a sample, such as birefringence. The contrast of OCT images may be enhanced by adding various contrast (scattering) agents into the tissue, which is analogous to using different stains in histology. Using the concepts of Doppler effect it is possible to simultaneously acquire tomographic images of tissue structure and blood flow [12].

4.1 Doppler OCT

The experimental setup for Doppler OCT does not vary from the one used for conventional OCT. Information about the velocity of scattering particles (such as blood cells in blood vessels) is retrieved by additional signal processing. This can be achieved using either TD-OCT or FD-OCT techniques. Derivation of the signal processing algorithm required for extracting the frequency shift information from OCT signal is beyond the scope of this seminar.

When scattering particles in the sample are moving, interference fringes in $I_{\mathrm{D}}(\tau)$ or $I_{\mathrm{D}}(\omega)$ change in time, because their distance from the beamsplitter (z_{S} equivalent) changes in time. In TD-OCT this results in change of the fringe frequency (see Eq. (10)). The center frequency ω_0 is modified by a Doppler frequency shift, which is proportional to the velocity component parallel to the incident beam, $\omega_{\mathrm{D}} = 4\pi v \cos\theta/\lambda$, where θ is the angle between the light beam and particle velocity v, and λ is the wavelength of the incident light. Note that this frequency shift is not directly connected to the Doppler effect for electromagnetic waves - the name was adopted by analogy. The flow velocity component parallel to the axis of the A-scan may be determined from the shift in the central frequency of the interference signal $I_{\mathrm{D}}(f)$. In TD-OCT this can be achieved by measuring how the modulation frequency of the signal fringes changes. This approach, however, limits the scan speeds and an alternative approach based on the change in phase instead of the frequency is available. Phase-resolved Doppler OCT enables both high velocity sensitivity and high A-scan rates.

When flow direction is perpendicular to the light beam, sensitivity for axial velocity is not sufficient to determine the flow velocity profile. Because the sample arm beam is broad before being focused to the sample, different parts of the beam will produce different Doppler shifts f_1 and f_2 (see Figure 5a) and consequently the spectrum of the measured interference signal will be additionally broadened. Transversal velocity can then be determined from the standard deviation of the spectrum

of the light at the detector. 3D flow velocity vector can be determined from multiple measurements of the scattering, but experimentally these measurements are performed simultaneously. Real time measurements with sensitivity on the order of 10 µm/s have been demonstrated [12].

Doppler OCT provides additional contrast from the velocity of particles in the sample (usually blood flow). This enables reliable differentiation of the vessel system from the surrounding tissues. This technique can be used to diagnose any disease that alters blood flow in the organs it affects.

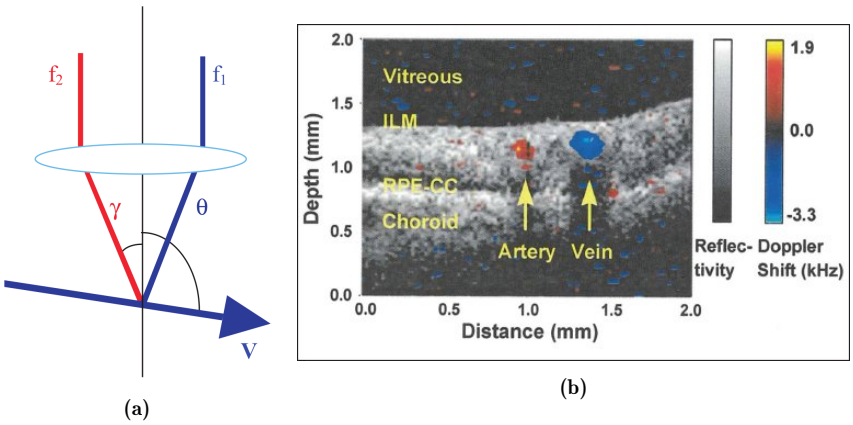

Figure 5. **(a)**: mechanism of transversal velocity measurement using Doppler shift broadening of the light source spectrum. **(b)**: The first demonstration of blood flow imaging in the living human eye, false-color overlay of Doppler signal on top of OCT image. Adapted from [12], [13].

5. Conclusion

Optical coherence tomography is an imaging technique which uses low coherence time of the light source to measure reflectivity from a spatially confined part within the sample. This enables construction of tissue reflectivity cross sections as well as 3D images of the samples.

OCT is especially attractive because of its non-invasive nature. It uses visible or near-infrared light, which does not damage the tissue, in contrast with imaging techniques based on ionizing radiation. High resolution of OCT enables accurate assessment of tissue morphology. The main disadvantage of OCT is its low imaging depth, which allows only imaging of the structures 1 - 2 mm below the surface.

Since its invention OCT has become a reliable tool in many medical specialties in both clinic and research. In ophthalmology, OCT has already become the standard for diagnostics. In other areas, additional sources of contrast are being developed to increase the diagnostic capabilities of OCT imaging. With its unique properties, optical coherence tomography is without a doubt an invaluable addition to the collection of medical imaging techniques.

REFERENCES

[1] D. J. Faber and T. G. van Leeuwen, "Optical coherence tomography," in *Optical-Thermal Response of Laser-Irradiated Tissue* (A. J. Welch and M. J. C. van Gemert, eds.), ch. 18, pp. 713–741, Springer Science & Business Media, 2011.

[2] D. W. and F. J. G., "Introduction to optical coherence tomography," in *Optical Coherence Tomography* (D. W. and F. J. G., eds.), ch. 1, pp. 1–45, Springer, Berlin, Heidelberg, 2008.

[3] "Michelson interferometer - wikipedia, the free encyclopedia." `https://en.wikipedia.org/wiki/Michelson_interferometer`. Accessed 4. 11. 2019.

[4] M. Čopič and M. Vilfan, "Fotonika." `https://jazbec.ijs.si/mvilfan/papers/Fotonika.pdf`. Accessed 28. 12. 2019.

[5] J. A. Izatt and M. A. Choma, "Theory of optical coherence tomography," in *Optical Coherence Tomography* (D. W. and F. J. G., eds.), ch. 2, pp. 47–72, Springer, Berlin, Heidelberg, 2008.

[6] H. D. Radhakrishnan S. and S. S., "Optical coherence tomography imaging of the anterior chamber angle," *Ophthalmology clinics of North America*, vol. 18, September 2005.

[7] Steven L. Jacques, "Optical properties of biological tissues: a review," *Phys. Med. Biol.*, vol. 58, May 2013.

[8] Huang, D., Swanson, E. A. et. al., "Optical coherence tomography," *Science*, vol. 254, no. 5035, pp. 1178–1181, 1991.

[9] J. F. de Boer, "Spectral/fourier domain optical coherence tomography," in *Optical Coherence Tomography* (D. W. and F. J. G., eds.), ch. 3, pp. 147–175, Springer, Berlin, Heidelberg, 2008.

[10] "Introduction to oct - obel." `http://obel.ee.uwa.edu.au/research/fundamentals/introduction-oct/`. Accessed 9. 12. 2019.

[11] Drexler W., Liu M., Kumar A. et. al., "Optical coherence tomography today: speed, contrast, and multimodality," *Journal of Biomedical Optics*, vol. 19, July 2014.

[12] C. Z. and Z. J., "Doppler optical coherence tomography," in *Optical Coherence Tomography* (D. W. and F. J. G., eds.), ch. 21, pp. 621–651, Springer, Berlin, Heidelberg, 2008.

[13] "Optical Coherence Tomography Angiography Algorithms | Ento Key." `https://entokey.com/optical-coherence-tomography-angiography-algorithms/`. Accessed 9. 12. 2019.